Proceedings of NCAD2008
NoiseCon2008-ASME NCAD
July 28-30, 2008, Dearborn, Michigan, USA

NCAD2008-73019

SOUND RADIATION FROM A PROPELLER IN A SUBMERGED RIB-STIFFENED DUCT

Wenlong Zhang
Department of Aerospace and Mechanical Engineering
University of Notre Dame
Notre Dame, IN 46556
Email: wzhang@nd.edu

Hafiz M. Atassi
Department of Aerospace and Mechanical Engineering
University of Notre Dame
Notre Dame, IN 46556
Email: atassi@nd.edu

ABSTRACT

This paper examines the interaction of nonuniform flows with propeller blades in a submerged elastic duct. The acoustic radiation from the duct is calculated and correlated to the flow nonuniformities and the propeller and duct characteristics. The case of a stiffened duct with ribs is also considered and the dispersion relation of the duct modes is compared with that of a regular duct. The dispersion relation of the stiffened duct has a periodic structure similar to that of connected oscillators with large number of independent modes. Because of our interest in the acoustic radiation of such a system, we focus our attention on the flexure modes. The model is first tested with simple internal forces such as monopoles and dipoles. The results for unstiffened ducts show strong directivity as the dipole radial location moves closer to the duct wall. For stiffened ducts, the magnitude of the acoustic response as well as the directivity vary strongly and show large peaks near the stiffened duct free modes. For a propeller, an Euler code provides the pressure distribution along the blades. This represents the dipole strength distribution. Its radiated sound is calculated by summing up the contribution of the distributed dipoles. In this process, compact source effects are also taken into account.

NOMENCLATURE

a shell radius
E Young's modulus
h shell thickness
m mode number
p pressure
P_{ef} far field acoustic radiated pressure
[S] stiffness matrix of shell
[R] inverse matrix of [S]
$\mathbf{U}$ velocity vector
c_1, c_2 speed sound in interior and exterior fluid
$J_{|m|}$ Bessel function
$H^{(1)}_{|m|}$ Hankel function of the first kind
$H^{(2)}_{|m|}$ Hankel function of the second kind
r_h hub radius
r_t tip radius
α axial wavenumber
α^* dimensionless axial wavenumber, $\alpha^* = \alpha a$
ν Poisson's ratio
ρ_1, ρ_2 interior and exterior densities
ρ_s shell material density
η damping factor
ζ_x, ζ_θ, ζ_r axial, circumferential and radial displacements
ω circular frequency
ω^* dimensionless frequency, $\omega^* = \omega a/c_2$

INTRODUCTION

The interaction of fluid and flexible structure gives rise to numerous physical problems and phenomena. The flexible structure is surrounded by the fluid, and fluid flow exerts pressure on the solid structure causing it to deform. For nonuniform flow, the structure vibrates in response to the unsteady fluid loading and

radiates sound in the surrounding fluid. In this paper, the coupling between nonuniform flow and a propeller in an elastic duct is modeled. The propeller is modeled as a rotor/stator stage. For simplicity, the duct is modeled as an infinite thin cylindrical shell with stiffened ribs for structural integrity.

The thin cylindrical shell has been studied by many researchers [1, 2] because it is a good theoretical model to study to give a better understanding of structural acoustics. A source in the cylindrical shell will generate several types of waves that propagate along the shell with associated disturbances in the fluid [3]. The dispersion equation shows that there are three propagating waves in the shell which correspond to flexure, compression and torsion waves. Analysis of the dispersion equation helps explain the acoustic radiation from the shell.

For the shell with no ribs, the flexural modes have short wavelength and do not radiate to the far field [4]. However, when the shell is stiffened by ribs, the flexure modes begin to radiate to the far field. When the shell is stiffened by periodically spaced identical ribs, the ribs exert meridional moments on the shell [5]. Bernblit [6, 7] developed a formulation to calculate the radiated sound from an infinite cylindrical shell, which is stiffened by periodic rings. Vasudevan [8] studied the sound radiation from a ribbed infinite cylindrical shell. It was found that the dispersion curves depend on the properties of the shell/rib system and the spacing between the ribs. Marcus *et al*. [9, 10] used finite-element modeling to study the radiated sound from the cylindrical shell with ribs. It was found that for higher circumferential mode numbers ($m > 10$), two structural resonances dominate the vibratory response of the shell. Rib thickness variations strongly affect the first pass band, while rib spacing variations strongly affect the second pass band.

Besides theoretical and numerical results, several experiments have been carried out for the cylindrical shell with ribs. Photiadis *.el.* [11] was among the first to experimentally study wave-number space response of a near periodically ribbed shell. The experimental results show a clear dispersion structure dominated primarily by the Bloch wave-number of flexural wave k and its replications by scattering from the periodic array, $k + 2\pi n/s$, where n is an integer, and s is the rib spacing. Sizable frequency gaps are typically a dominant feature of the results.

Structural acoustics focuses on assumed sources of noise, such as, single force, monopole, dipoles. When sound radiation from a propeller is investigated, the source of noise is obtained from the propeller-duct system. The propeller, which works with incoming nonuniform flow, is modeled as a rotor/stator stage. Because of the rotor rotation, it is necessary to represent the propagation of upstream disturbances in a swirling mean flow [12]. For a uniform flow, the pressure and vorticity are uncoupled. For a swirling mean flow, Atassi *et al*. [12, 13] developed a model for the representation of upstream disturbances and their interaction with a row of blades. The results showed that the swirling flow may strongly affect the acoustic and vortical spectral composition of propagating modes in the duct.

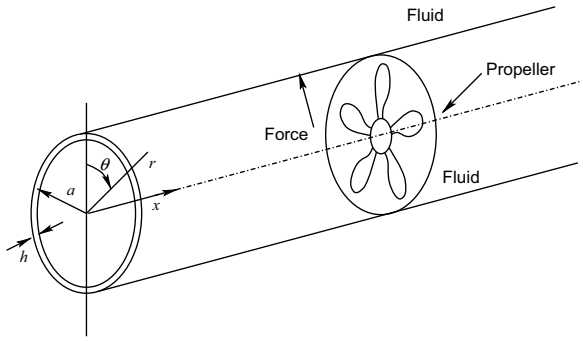

Figure 1. Geometry of cylindrical shell excited by point force.

In this paper, we examine the effects of an elastic duct on the sound radiation from a propeller inside the duct. The coupling of the duct motion to the propeller generated flow is implemented using Euler's equations and the shell equations which are coupled by the boundary condition between the fluid and the shell. To our best knowledge, this coupling is new.

This paper is organized as follows. First, the governing equations of the shell and rib motions and linearized Euler equations of fluid motion are presented. Then, we examine the effects of the radial location and direction of a single dipole on the sound pressure level radiated by the duct. These results are correlated with the dispersion curves for both the duct and the rib-stiffened duct. For a propeller, the unsteady pressure along the blades is obtained from [12]. This unsteady pressure represents the strength of the dipole distribution and direction along the blades. The radiated sound pressure due to the propeller is then calculated for an aluminum duct. Finally, we summarize our results in the conclusions.

MATHEMATICAL FORMULATIONS

In this paper, the thin cylindrical shell is surrounded by water in a cylindrical coordinate system (x, θ, r). The geometry is shown in figure 1 . The motion of thin cylindrical shell is described by Goldenveizer & Novozhilov equations [5]. The shell equations are a system of three linear equations, the first is of order 2, the second is of order 3, and the third of order 4. We consider a single harmonic excitation, $e^{-i\omega t}$, of frequency ω, and use Fourier transform,

$$F(r,\theta,x) = \frac{1}{2\pi}\sum_{m=-\infty}^{m=+\infty} e^{im\theta}\int_{-\infty}^{+\infty} f(r,m,\alpha)e^{i\alpha x}d\alpha, \qquad (1)$$

$$f(r,m,\alpha) = \frac{1}{2\pi}\int_{0}^{2\pi} e^{-im\theta}\int_{-\infty}^{+\infty} F(r,\theta,x)e^{-i\alpha x}dxd\theta, \qquad (2)$$

where m is the circumferential mode number and α is the axial wave number. $F(r,\theta,x)$ is the field quantity and $f(r,m,\alpha)$ is the spectral field quantity. Thus, the spectral equations of shell motions with interior and exterior fluid loading are given by,

$$\begin{pmatrix} S_{11} & S_{12} & S_{13} \\ S_{21} & S_{22} & S_{23} \\ S_{31} & S_{32} & S_{33}+F_l \end{pmatrix} \begin{pmatrix} \zeta_x(m,\alpha) \\ \zeta_\theta(m,\alpha) \\ \zeta_r(m,\alpha) \end{pmatrix} = \begin{pmatrix} e_x(m,\alpha) \\ e_\theta(m,\alpha) \\ e_r(m,\alpha) \end{pmatrix}, \quad (3)$$

where, the amplitudes $\zeta_x(m,\alpha)$, $\zeta_\theta(m,\alpha)$, $\zeta_r(m,\alpha)$ are the spectral displacements; the amplitudes $e_x(m,\alpha)$, $e_\theta(m,\alpha)$, $e_r(m,\alpha)$ are the spectral excitations.

The elements in the stiffness matrix $[S]$ are given by,

$$S_{11} = E_1\left(\alpha^2 + m^2\frac{1-\nu}{2a^2}\right) - \omega^2\rho_s h,$$

$$S_{12} = E_1(1+\nu)\frac{m\alpha}{2a},$$

$$S_{13} = -iE_1\nu\frac{\alpha}{a}, \qquad S_{21} = S_{12},$$

$$S_{22} = E_1\left[\frac{(1-\nu)\alpha^2}{2} + \frac{m^2}{a^2} + 2\alpha^2\beta^2(1-\nu) + \frac{\beta^2 m^2}{a^2}\right] - \omega^2\rho_s h,$$

$$S_{23} = -iE_1\left[\frac{m}{a^2} + \beta^2(2-\nu)\alpha^2 m + \frac{\beta^2 m^3}{a^2}\right],$$

$$S_{31} = -S_{13}, \qquad S_{32} = -S_{23},$$

$$S_{33} = E_1\left[\frac{1}{a^2} + \frac{\beta^2 m^4}{a^2} + \alpha^4\beta^2 a^2 + 2\beta^2 m^2\alpha^2\right] - \omega^2\rho_s h.$$

In these equations, $E_1 = \frac{Eh}{1-\nu^2}$, where, E is Young's Modulus, ν is Poisson's ratio, ρ_s is the shell's density, h is the thickness of the cylindrical shell, a is the shell's mean radius, and $\beta^2 = \frac{h^2}{12a^2}$.

Note that S_{ij} do not contain the effect of fluid loading. This term denoted F_l in Eq. (3) has the following expression for both the inner and outer fluid loading,

$$F_l = -\frac{\rho_1\omega^2}{\gamma_1}\frac{H^{(1)}_{|m|}(\gamma_1 a)H^{'(2)}_{|m|}(\gamma_1 r_h) - H^{'(1)}_{|m|}(\gamma_1 r_h)H^{(2)}_{|m|}(\gamma_1 a)}{H^{'(1)}_{|m|}(\gamma_1 a)H^{'(2)}_{|m|}(\gamma_1 r_h) - H^{'(1)}_{|m|}(\gamma_1 r_h)H^{'(2)}_{|m|}(\gamma_1 a)} + \frac{\rho_2\omega^2 H^{(1)}_{|m|}(\gamma_2 a)}{\gamma_2 H^{'(1)}_{|m|}(\gamma_2 a)}, \quad (4)$$

where r_h is hub radius, $J_{|m|}$ is Bessel function, $H^{(1)}_{|m|}$ and $H^{(1)}_{|m|}$ are Hankel functions of the fist kind and the second kind, respectively. $\gamma_1 = \sqrt{k_1^2 - \alpha^2}$, $k_1 = \omega/c_1$, and c_1 is the interior fluid sound speed. $\gamma_2 = \sqrt{k_2^2 - \alpha^2}$, $k_2 = \omega/c_2$, and c_2 is the exterior fluid sound speed. ρ_1 and ρ_2 are the interior and exterior fluid densities, respectively.

When $r_h = 0$, the fluid loading term becomes,

$$F_l = -\rho_1\omega^2\frac{J_{|m|}(\gamma_1 a)}{\gamma_1 J'_{|m|}(\gamma_1 a)} + \rho_2\omega^2\frac{H^{(1)}_{|m|}(\gamma_2 a)}{\gamma_2 H^{'(1)}_{|m|}(\gamma_2 a)}. \quad (5)$$

The spectral response of the elastic cylindrical shell without ribs is given by Eq. (3). The solutions of the shell displacements can be obtained by simple matrix inversion from Eq. (3),

$$\begin{pmatrix} \zeta_x(m,\alpha) \\ \zeta_\theta(m,\alpha) \\ \zeta_r(m,\alpha) \end{pmatrix} = \begin{pmatrix} R_{11} & R_{12} & R_{13} \\ R_{21} & R_{22} & R_{23} \\ R_{31} & R_{32} & R_{33} \end{pmatrix} \begin{pmatrix} e_x(m,\alpha) \\ e_\theta(m,\alpha) \\ e_r(m,\alpha) \end{pmatrix}. \quad (6)$$

A structural damping is introduced to avoid singular behavior where Young's Modulus E is replaced by E_c,

$$E_c = E(1-i\eta),$$

where η is the damping factor.

A rib is assumed to run circumferentially around the shell and is schematically shown in Figure 2. The rib is assumed to exert a meridional moment on the shell, so the shell equation should be expanded to include moment excitation per unit area $M_\theta(m,\alpha)$ [5]. The expanded matrix relation for the shell with ribs is given by,

$$\begin{pmatrix} \zeta_x(m,\alpha) \\ \zeta_\theta(m,\alpha) \\ \zeta_r(m,\alpha) \\ \psi_\theta(m,\alpha) \end{pmatrix} = \begin{pmatrix} R_{11} & R_{12} & R_{13} & R_{14} \\ R_{21} & R_{22} & R_{23} & R_{24} \\ R_{31} & R_{32} & R_{33} & R_{34} \\ R_{41} & R_{42} & R_{43} & R_{44} \end{pmatrix} \begin{pmatrix} F_{ex} \\ F_{e\theta} \\ F_{er} \\ M_\theta \end{pmatrix}, \quad (7)$$

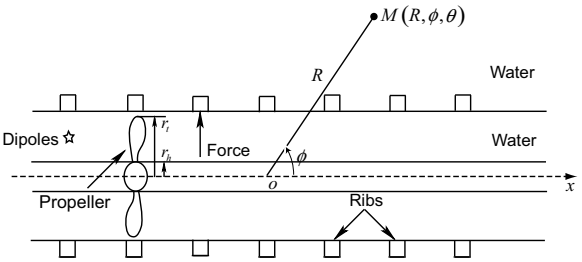

Figure 2. Schematic of a rib-stiffened cylindrical shell. M is the observer point in the spherical coordinate system. R is the distance between the source and observer, θ is the polar angle, and ϕ is the azimuthal angel.

where,

$$R_{14} = -i\alpha R_{13}, \qquad R_{24} = -i\alpha R_{23}, \qquad R_{34} = -i\alpha R_{33},$$
$$R_{41} = i\alpha R_{31}, \qquad R_{42} = i\alpha R_{32}, \qquad R_{43} = i\alpha R_{33},$$
$$R_{44} = \alpha^2 R_{33}.$$

The spectral displacement of shell with ribs is obtained as [5],

$$\begin{aligned}\{\zeta(m,\alpha)\} = \; & [R(m,\alpha)]\{F_e(m,\alpha)\} - \frac{1}{s}[R(m,\alpha)][B(m)] \times \\ & \left[[I] + \frac{1}{s}\sum_{q=-\infty}^{q=\infty}[R(m,\alpha+2\pi q/s)][B(m)]\right]^{-1} \\ & \times \sum_{q=-\infty}^{q=\infty}[R(m,\alpha+2\pi q/s)] \\ & \{F_e(m,\alpha+2\pi q/s)\}, \end{aligned} \tag{8}$$

where s is the rib spacing, $\{F_e\}$ is the excitation, and q is the number of ribs. Matrix B is a 4×4 dynamics stiffness matrix, which connects the forces and displacements at cylinder attachment points.

For a given source excitation, the spectral displacements $\zeta(m,\alpha)$ can be numerically solved by Eq. (8). Using the stationary phase method, we derive the following expression of the far field acoustic radiated pressure in a spherical coordinate system (R,ϕ,θ),

$$P_{ef} = \frac{-i\rho\omega^2 e^{ikR}}{\pi kR\sin\phi}\sum_{m=-\infty}^{m=+\infty}\frac{(-i)^{|m|}\zeta_r(m,\alpha_0)}{H'^{(1)}_{|m|}(ka\sin\phi)}e^{im\theta}, \tag{9}$$

where $\alpha_0 = k\cos\phi$ is the stationary phase wavenumber.

The fluid motion is governed by the conservation laws of mass, momentum, and energy, and we use the Euler equations as the governing equations [14],

$$\frac{D\rho}{Dt} + \rho\nabla\cdot\mathbf{U} = 0, \tag{10}$$

$$\rho\frac{D\mathbf{U}}{Dt} = -\nabla p, \tag{11}$$

where ρ, $\mathbf{U}$, and p are the density, velocity, and pressure of the fluid, respectively, and $\frac{D}{Dt}$ is the material derivative defined by,

$$\frac{D}{Dt} \equiv \frac{\partial}{\partial t} + \mathbf{U}\cdot\nabla. \tag{12}$$

We can linearize the governing equations about the steady mean flow quantities by writing,

$$\mathbf{U}(\mathbf{x},t) = \mathbf{U}_0(\mathbf{x}) + \mathbf{u}(\mathbf{x},t), \tag{13}$$

$$p(\mathbf{x},t) = p_0(\mathbf{x}) + p'(\mathbf{x},t), \tag{14}$$

$$\rho(\mathbf{x},t) = \rho_0(\mathbf{x}) + \rho'(\mathbf{x},t), \tag{15}$$

where $\mathbf{x}$ stands for the position vector, t for time, and ρ_0, $\mathbf{U_0}$, and p_0 are the steady density, velocity, and pressure of the fluid, respectively, and ρ', $\mathbf{u}$, and p' are the corresponding unsteady perturbation quantities such that

$$|\mathbf{u}(\mathbf{x},t)| \ll |\mathbf{U}_0(\mathbf{x})|, \tag{16}$$

$$|p'(\mathbf{x},t)| \ll |p_0(\mathbf{x})|, \tag{17}$$

$$|\rho'(\mathbf{x},t)| \ll |\rho_0(\mathbf{x})|. \tag{18}$$

Thus, the first-order continuity, momentum and energy equations resulting from the linearization are given,

$$\frac{D_0\rho'}{Dt} + (\mathbf{u}\cdot\nabla)\rho_0 + \rho_0\nabla\cdot\mathbf{u} + \rho'\nabla\cdot\mathbf{U}_0 = 0, \tag{19}$$

$$\rho_0 \left(\frac{D_0 \mathbf{u}}{Dt} + (\mathbf{u} \cdot \nabla)\mathbf{U}_0 \right) + \rho'(\mathbf{U}_0 \cdot \nabla \mathbf{U}_0) = -\nabla p'. \qquad (20)$$

The boundary condition at the hub is given by,

$$\left(\frac{\partial u_r}{\partial r} \right)_{r_h} = 0. \qquad (21)$$

The boundary condition at the inner surface of the duct is given by,

$$u_r = \frac{D_0 \zeta_r}{Dt}. \qquad (22)$$

NUMERICAL RESULTS

In this section, numerical results are presented for the far field sound pressure level of the acoustic radiation from an infinite aluminum cylindrical shell which is filled and submerged with water. The sound pressure level is defined as $20\log_{10}\lim_{R\to\infty}|RP_{ef}(R,\phi,\theta)|+120$, corresponding to reference pressure of 1 micro-pascal. We define the non-dimensional variables of wavenumber and frequency as, $\alpha^* = \alpha a$, and $\omega^* = \frac{\omega a}{c_2}$, where a is the radius of the shell and $c_2 = 1482 m/s$ is the speed of sound in water. The following parameters for the shell and rib were used in the numerical calculations. The aluminum cylindrical shell has radius $1.0m$ and thickness $0.01m$. The steel rib dimensions are depth $0.06m$ and width $0.06m$. The rib spacing is $1.0m$. The structural damping, $\eta = 0.02$, is introduced.

Dispersion Curves

The dispersion relation is the relation between frequency and wavenumber for which the resonance occurs. For a shell with no ribs, the dispersion equation is simply,

$$\begin{vmatrix} S_{11} & S_{12} & S_{13} \\ S_{21} & S_{22} & S_{23} \\ S_{31} & S_{32} & S_{33}+F_l \end{vmatrix} = 0, \qquad (23)$$

Note that although S_{12}, S_{21}, S_{13}, and S_{31} depend on α while the other coefficients of Eq. (23) depend on α^2, the determinant itself depends on even powers of α ensuring a symmetry about $\alpha = 0$ with respect to the wavenumber. By solving the dispersion equation, we find there are three propagating waves in the shell which correspond to flexure, compression and torsion waves. We are interested in the flexure waves because the flexure waves are related with the radiated sound, and the curves of the flexure waves can be used to explain the strong acoustic radiation from the shell.

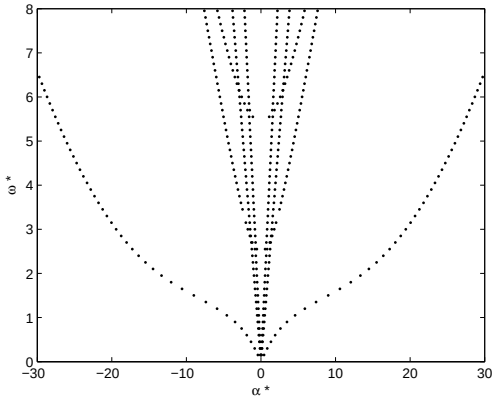

Figure 3. Wavenumber versus frequency dispersion plot of a water-filled Aluminum shell surrounded by a vacuum, for circumferential harmonic m=0.

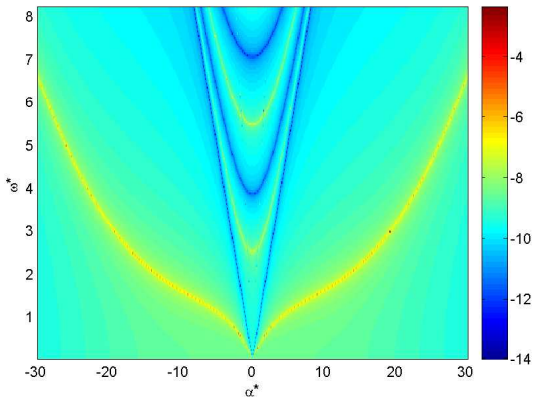

Figure 4. Flexure waves of a water-filled Aluminum cylinder surrounded by a vacuum excited by a unit force, for circumferential harmonic m=0. The color scale represents the log_{10} displacement value in meters.

Figure 3 presents the dispersion curves of a water-filled Aluminum shell surrounded by a vacuum for circumferential harmonic m=0, which is obtained by finding the roots of the dispersion equation. The two outside branches in figure 3 are the flexure waves. Figure 4 shows the radial displacements of a water-filled Aluminum shell surrounded by a vacuum for circumferential harmonic m=0, which is obtained by calculating the radial displacements excited by a unit radial traction (force per unit area). When the radial displacements representing flexural modes are large, they indicate resonant conditions. Figure 4 shows this representation for a simple shell (no ribs) and is compared for validation with figure 3 calculated analytically.

The dispersion equation for the rib-stiffened duct is only

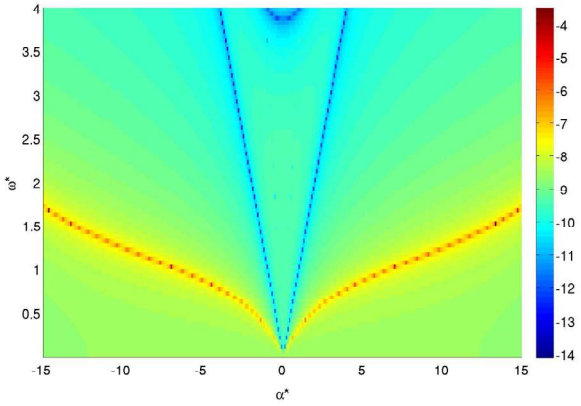

Figure 5. Flexure waves of a water-filled Aluminum shell surrounded by water for circumferential harmonic m=0, which is excited by a unit force. The color scale represents the log_{10} displacement value in meters.

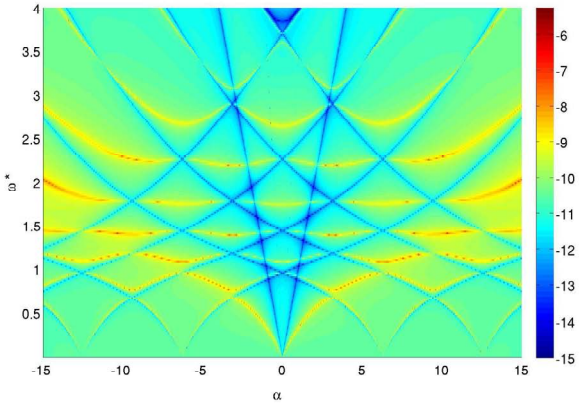

Figure 6. Flexure waves of a water-filled Aluminum ribbed shell surrounded by water for circumferential harmonic m=0, which is excited by a unit force. The color scale represents the log_{10} displacement value in meters.

known numerically. We apply a single radial force at the duct boundary and solve for the radial displacements. Figure 5 shows the flexure waves of a water-filled aluminum unribbed shell surrounded by water for circumferential harmonic m=0. We see that the yellow branches are the flexure waves. Figure 6 presents the flexure waves of a water-filled aluminum ribbed shell surrounded by water for circumferential harmonic m=0. Comparing the two figures, it is seen that when the cylindrical shell is stiffened by ribs, the ribs strongly change the dispersion curves and lead to free modes with much smaller wavelength. We also find that for the shell without ribs, there are always free flexure modes for all the frequencies. But, for the shell with ribs, there are no free flexure modes for some frequency zones, which means that the far field radiated sound is very weak for these frequencies. Those zones are called silence zones. And the control ribs can be used to reduced noise for some frequencies.

We also calculate the flexure waves for higher mode numbers, $m = 5, 8$, and the results are shown in figure 7 and 8, respectively. For different mode numbers, the flexure curves are different and the locations of silence zones are different too. These results clearly show the strong influence of the ribs on the radiated sound. Further examination is underway for the nature of flexure waves and their possible interaction with acoustic modes for frequencies below the coincidence frequency.

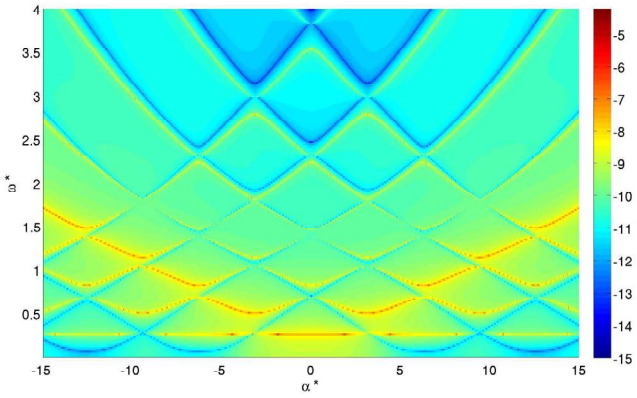

Figure 7. Flexure waves of a water-filled Aluminum ribbed shell surrounded by water for circumferential harmonic m=5, which is excited by a unit force. The color scale represents the log_{10} displacement value in meters.

Mechanical Point Force Excitation

We have used a radial point force excitation to determine the dispersion relation. Here, we show the broadside far field sound pressure levels in figure 9. Comparing the far field sound pressure level of the shell with ribs and that of the shell without ribs, we find that the control ribs strongly change the far field sound radiations. The peaks in the spectrum can be associated with the flexure waves in the shell. At some frequencies, the sound level of ribbed shell is much lower than that of unribbed shell, the reason could be the cancellation between the waves due to control ribs.

Figure 10 shows 45^o off broadside far field sound pressure levels when the excitation is a unit radial force. Again, we can find that the control ribs strongly change the far field sound radiations.

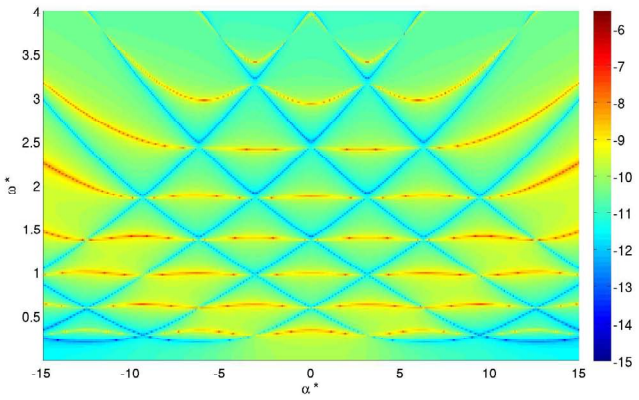

Figure 8. Flexure waves of a water-filled Aluminum ribbed shell surrounded by water for circumferential harmonic m=8, which is excited by a unit force. The color scale represents the log_{10} displacement value in meters.

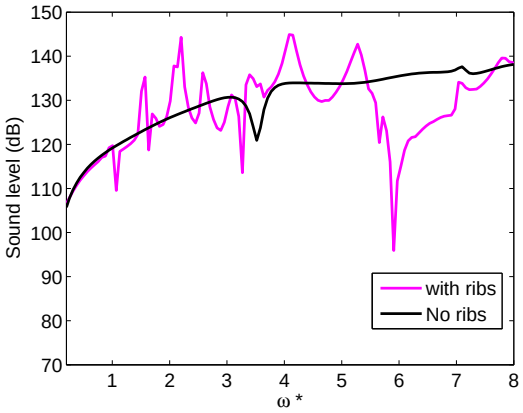

Figure 9. Far field sound pressure levels at broadside ($\phi = \pi/2, \theta = 0$) of ribbed and unribbed cylindrical shells caused by a unit radial point force.

Monopole Excitation

In this part, the excitation is considered as a monopole located at different radial positions, $r_0 = 0.1a, 0.3a, 0.5a$ and $0.8a$. The radiated sound pressure is normalized to the free field pressure of a monopole.

Figures 11 and 12 show the far field sound pressure levels of the unribbed and ribbed cylindrical shells by a monopole at the observation angle $\phi = \pi/3$, respectively. It is seen that the radial locations of the monopole do not have much effects on the far field sound radiation. Because of the interaction with the control ribs, the flexure modes cause significant change to the radiated sound. The peaks in the spectrum can be associated with the flexure modes in the flexure curves.

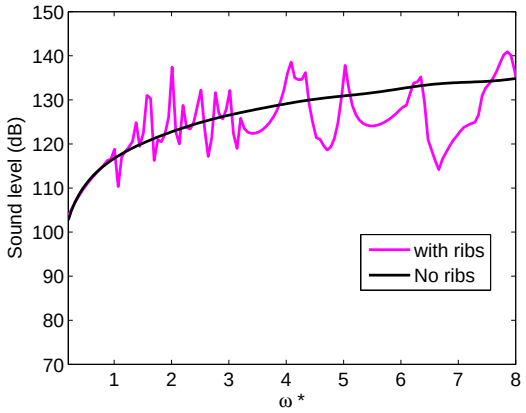

Figure 10. Far field sound pressure levels at 45^o off broadside ($\phi = \pi/4, \theta = 0$) of ribbed and unribbed cylindrical shells caused by a unit radial point force.

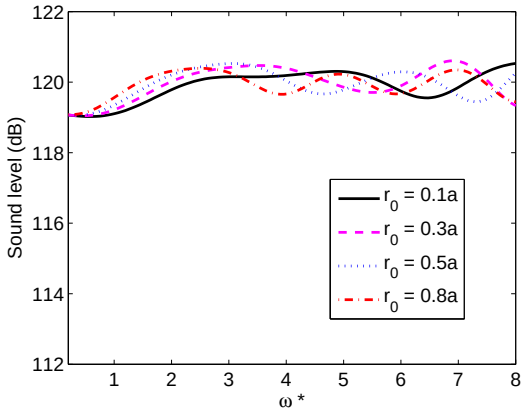

Figure 11. Far field sound pressure levels at $\phi = \pi/3$ of the unribbed cylindrical shell caused by a monopole.

Dipole Excitation

In this part, the excitations are considered as axial, radial, and circumferential dipoles. We put the dipoles at different radial locations, $r_0 = 0, 0.1a, 0.3a, 0.5a$ and $0.8a$. Two observation angles are chosen for different values of ϕ. The radiated sound pressure is normalized to the free field pressure of a dipole.

Figure 13 shows the far field sound pressure levels of the unribbed cylindrical shell caused by axial dipoles at the observation angle $\phi = \pi/3$. It is seen that the farfield sound radiation depends on the radial location of axial dipoles. When ω^* is less than 3.5, the far field sound level increases as the location of the dipoles changes from $r_0 = 0.0$ to $r_0 = 0.8a$. But, when ω^* is more than 3.5, the far field sound levels of axial dipoles located at $r_0 = 0.5a$ and $r_0 = 0.8a$, decrease as the frequency increases. Figure 14

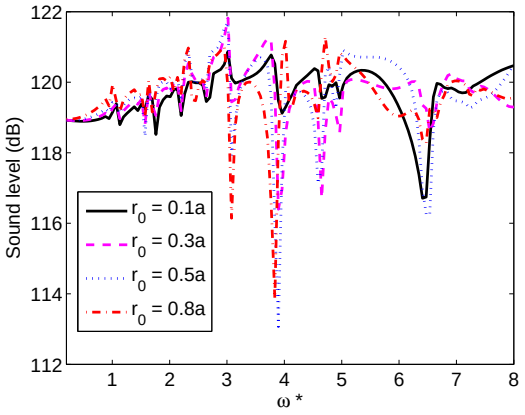

Figure 12. Far field sound pressure levels at $\phi = \pi/3$ of the ribbed cylindrical shell caused by a monopole.

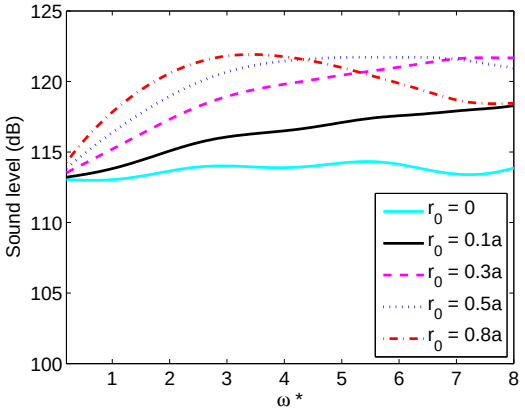

Figure 13. Far field sound pressure levels at $\phi = \pi/3$ of the unribbed cylindrical shell caused by an axial dipole.

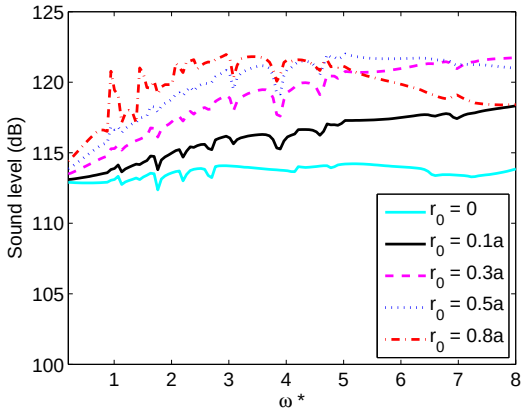

Figure 14. Far field sound pressure levels at $\phi = \pi/3$ of the ribbed cylindrical shell caused by axial dipoles.

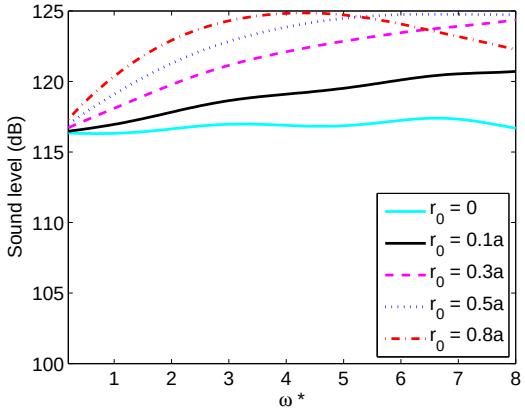

Figure 15. Far field sound pressure levels at $\phi = \pi/4$ of the unribbed cylindrical shell caused by axial dipoles.

shows the far field sound pressure levels of the ribbed cylindrical shell caused by axial dipoles at the observation point $\phi = \pi/3$. The control ribs change the far field sound level. The peaks in the plot occur near the shell flexure modes.

Figures 15 and 16 show the far field sound pressure levels of the unribbed and ribbed cylindrical shells caused by axial dipoles at the observation angle $\phi = \pi/4$. The results are similar to figure 13 and 14 and do not exhibit the strong dependence of the observation angle ϕ observed in figures 9 and 10. It is noticed that the far field sound level increases about 9 dB as the location of axial dipole moves from the axis of the shell to $r_0 = 0.8a$.

Figures 17 and 18 shows the far field sound pressure levels of the unribbed and ribbed cylindrical shells caused by circumferential dipoles at the observation angle $\phi = \pi/2$. Figures 19 and 20 shows the far field sound pressure levels of the unribbed and ribbed cylindrical shells caused by circumferential dipoles at the observation angle $\phi = \pi/4$. From these figures, it is found that the far field sound level increases as the location of the dipole changes from $r_0 = 0$ to $r_0 = 0.8a$, which means the circumferential dipole has stronger effect on the far field sound radiation when the location of the circumferential dipole is closer to the cylindrical shell.

Figures 21 and 22 show the far field sound pressure levels of the unribbed and ribbed cylindrical shells caused by radial dipoles at the observation angle $\phi = \pi/2$. It is observed that the far field sound levels decrease as the location of radial dipoles changes from $r_0 = 0.0$ to $r_0 = 0.8a$. The results of the far field sound pressure levels of unribbed and ribbed cylindrical shells caused by radial dipoles at the observation angle $\phi = \pi/4$ are shown in figures 23 and 24, respectively. We note that as the

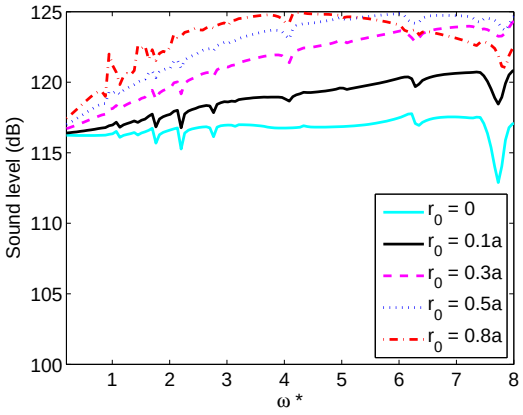

Figure 16. Far field sound pressure levels at $\phi = \pi/4$ of the ribbed cylindrical shell caused by axial dipoles.

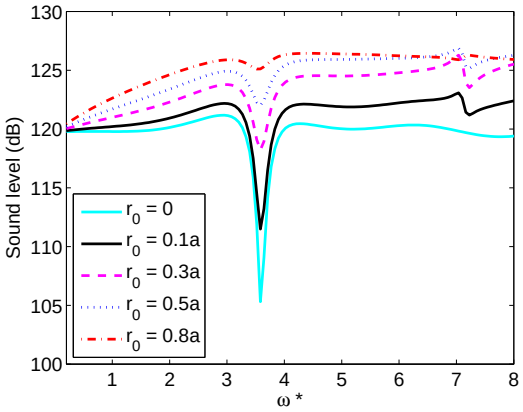

Figure 17. Far field sound pressure levels at $\phi = \pi/2$ of the unribbed cylindrical shell caused by circumferential dipoles.

radial dipoles move toward the shell, the far field sound level is reduced. This is contrary to the results of axial and circumferential dipoles. These results have been checked and we do not have a simple explanation for this behavior.

The results of the sound pressure level radiated from a dipole inside a duct with or without ribs clearly show strong dependence of the sound pressure level on the radial position of the dipole and its orientation. Figures 13 to 24 show sound pressure level radiations can reach more than 10 dB. These results demonstrate the inadequate assumption often used in structural acoustics wherein distributed dipole sources are treated as a single "blocked dipole" when the acoustic transfer function is calculated.

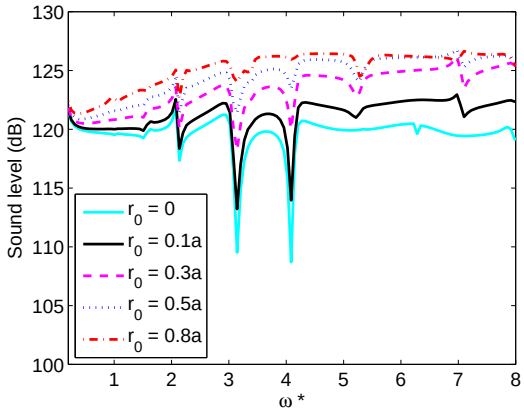

Figure 18. Far field sound pressure levels at $\phi = \pi/2$ of the ribbed cylindrical shell caused by circumferential dipoles.

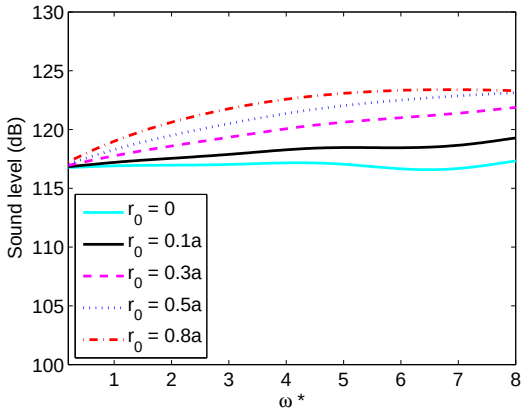

Figure 19. Far field sound pressure levels at $\phi = \pi/4$ of the unribbed cylindrical shell caused by circumferential dipoles.

Coupling the Propeller with the Shell

In this part, we present preliminary results for nonuniform flow interaction with a propeller in an elastic duct. The boundary conditions are as follows. A quasi-periodicity condition is implemented circumferentially. This implies a quasi-periodic dependence on θ of the form $e^{im\theta}$, where $m = 2\pi n/B$, where n is an integer and B is the number of propeller blades. Non-reflecting boundary conditions are imposed at the inlet and outlet. The boundary conditions at the hub radius and on the stator's surfaces are impermeability condition. At the duct wall, the boundary condition is given by Eq. (22). As an example for the preliminary results we present, the number of rotor blades is 2 and the number of the stator blades is 10. The mean-flow total Mach number is $M = 0.05$ and the hub-tip ratio is 0.6. We choose frequency $\omega^* = 1$ and use a grid of $\{n_x \times n_\theta \times n_r\} = \{121 \times 41 \times 41\}$. The

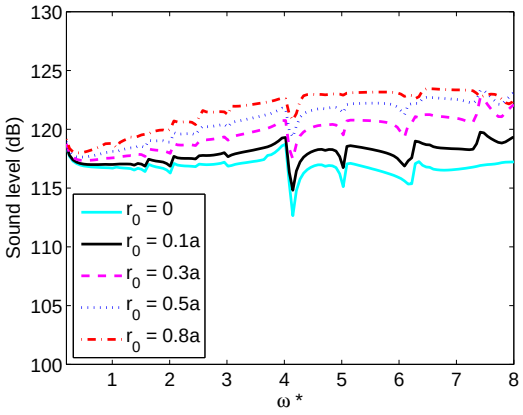

Figure 20. Far field sound pressure levels at $\phi = \pi/4$ of the ribbed cylindrical shell caused by circumferential dipoles.

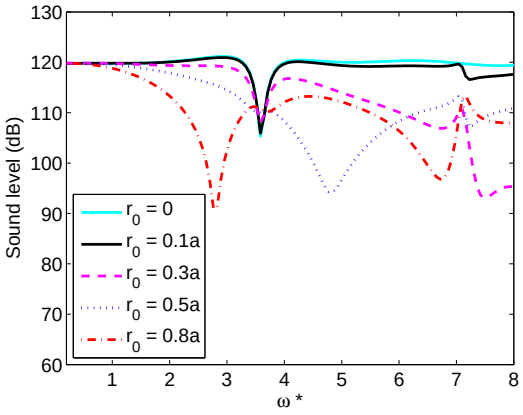

Figure 21. Far field sound pressure levels at $\phi = \pi/2$ of the unribbed cylindrical shell caused by radial dipoles.

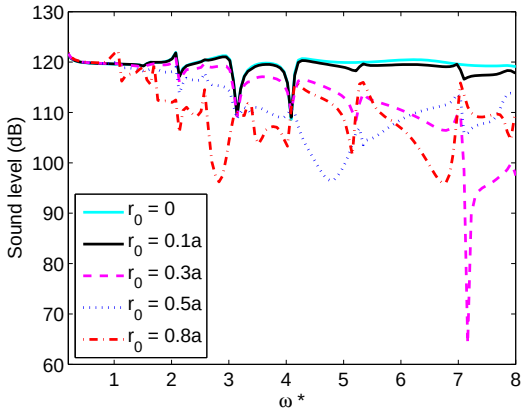

Figure 22. Far field sound pressure levels at $\phi = \pi/2$ of the ribbed cylindrical shell caused by radial dipoles.

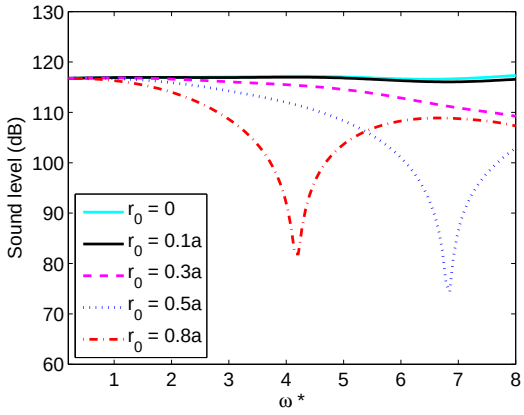

Figure 23. Far field sound pressure levels at $\phi = \pi/4$ of the unribbed cylindrical shell caused by radial dipoles.

material of the duct is aluminum.

Figure 25 shows the real and imaginary parts of the duct wall displacements in response to the unsteady pressure excitations of rotor-stator interaction assuming a rigid wall when computing the blade unsteady pressure. The wall displacements are non-dimensionalized with respect to the radius of the duct. Figure 26 shows the duct wall displacements in response to unsteady pressure excitations of rotor-stator interaction assuming an elastic wall when computing the blade unsteady pressure. For the rigid wall, there are no propagating acoustic waves in the duct. On the other hand, for the elastic wall, there are three propagating acoustic waves corresponding to mode numbers, $m = 12, 2, -8$. This accounts for the larger wall displacements shown in figure 26.

Figure 27 shows a polar plot of the sound pressure directivity of the rigid wall and elastic wall excitations. The acoustic pressure is non-dimensionalized with respect to $\rho_2 U_x u_g$, where U_x is mean velocity in x direction, and u_g is the gust upwash. For the present results, $u_g = 0.1U_x$. For the rigid wall excitation, the peak value of the pressure is 0.037, for the elastic wall excitation, the peak value of the pressure is 0.048. The acoustic pressure is enhanced when the elastic duct is coupled to the propeller by more than 2 dB.

CONCLUSIONS

The results of a numerical study of the far field sound radiation from an infinite thin cylindrical shell with control ribs are reported here.

It is found that when the cylindrical shell is stiffened by the

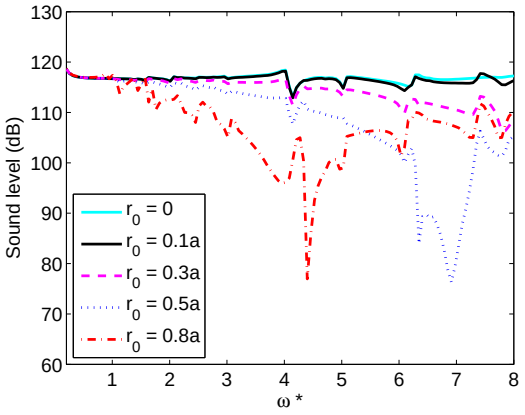

Figure 24. Far field sound pressure levels at $\phi = \pi/4$ of the ribbed cylindrical shell caused by radial dipoles.

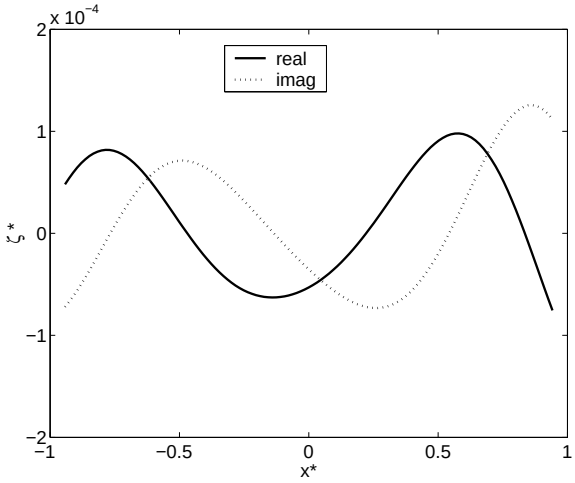

Figure 25. The real and imaginary parts of the duct wall displacements in response to rotor-stator interaction by the rigid wall excitation. The displacement is normalized to the duct mean radius in meters.

ribs, the control ribs strongly change the dispersion curves, and the silence zones are found for the shell with ribs. This suggests that control ribs can be used to reduce noise for some frequencies.

When the source excitation is a radial point force, the control ribs strongly change the far field sound radiations. The peaks in the spectrum are associated with the flexure waves in the shell. And for some frequencies the far field sound level can be reduced by the cancellation between the waves due to the control ribs.

For different radial positions of a monopole in a rib-stiffened duct, the locations of the peaks in the spectrum are almost same, although the magnitude are different. The peaks in the spectrum

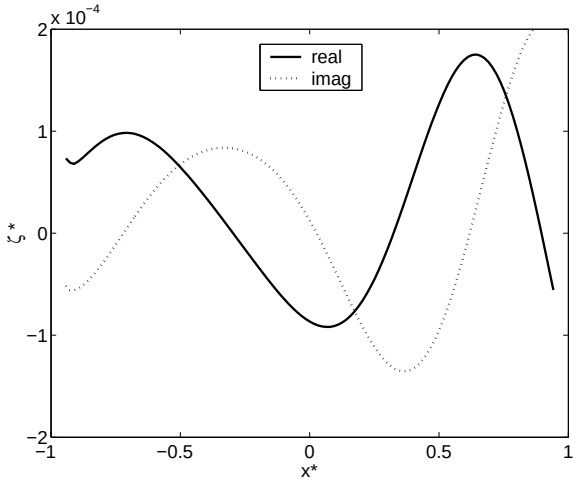

Figure 26. The real and imaginary parts of the duct wall displacements in response to rotor-stator interaction by the elastic wall excitation. The displacement is normalized to the duct mean radius in meters.

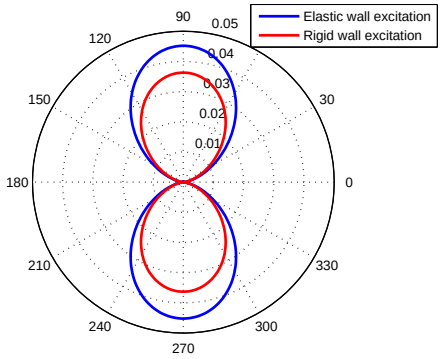

Figure 27. Comparison of sound pressure directivity of the aluminum duct between the rigid wall excitation and the elastic wall excitation. The acoustic pressure is non-dimensionalized with respect to $\rho_2 U_x u_g$, where U_x is mean velocity in x direction, and u_g is the gust upwash, $u_g = 0.1U_x$.

are associated with the flexure modes in the flexure curves.

For dipoles, the radial positions significantly change the sound pressure level for the axial, radial and circumferential orientations.

Preliminary results for the coupling between the propeller and the elastic duct are presented. It is founded that the elasticity of the shell enhances the acoustic sources and add more than 2 dB to the radiated acoustics pressure. The results suggest that for different combinations of rotor/stator blade counts, it is possible

to have low circumferential mode number, which is an efficient radiator of acoustic energy. The results also indicate that when free shell modes exist, we have propagating shell modes which force acoustic modes inside the duct and yield higher acoustic radiation outside the duct.

ACKNOWLEDGMENT

The research is supported by a grant No. N000140710647 P0001 of the Office of Naval Research.

REFERENCES

[1] Fuller, C. R., and Fahy, F. J., 1982. "Characteristics of wave propagation and energy distributions in cylindrical elastic shells filled with fluid". *Journal of Sound and Vibration,* **81(4)**, pp. 501–518.

[2] Scott, J. F., 1988. "The free modes of propagation of an infinite fluid-loaded thin cylindrical shell". *Journal of Sound and Vibration,* **125(2)**, pp. 241–280.

[3] Brazier-Smith, P. R., and Scott, F. M., 1985. "On the determination of the roots of dispersion equations by use of winding number integrals". *Journal of Sound and Vibration,* **145(3)**, pp. 503–510.

[4] Photiadis, D. M., and Bucaro, J., 2000. "Resonant response of complex shell structures". *Journal of the Acoustical Society of America,* **108(3)**, pp. 1027–1035.

[5] Skelton, E. A., and James, J. H., 1997. *Theoretical Acoustics of underwater structures*. Imperial College Press.

[6] Bernblit, M. V., 1976. "Sound radiation from a ribbed cylindrical shell". *Sov. Phys. Acoust.,* **21(6)**, pp. 518–521.

[7] Bernblit, M. V., 1975. "Sound radiation by a thin elastic cylindrical shell with reinforced ribs". *Sov. Phys. Acoust.,* **20(5)**, pp. 414–418.

[8] Vasudevan, R., 1994. Sound radiation from a coated/ribbed/layered infinite cylindrical shell. CDNSWC-SIG 93/226-725.

[9] Marcus, M. H., and Houston, B. H., 2000. "Wave localization on a submerged cylindrical shell with rib aperiodicity". *Journal of the Acoustical Society of America,* **109(3)**, pp. 865–869.

[10] Marcus, M. H., and Houston, B. H., 2002. "The effect of internal point masses on the radiation of a ribbed cylindrical shell". *Journal of the Acoustical Society of America,* **112(3)**, pp. 961–965.

[11] Photiadis, D. M., and Williams, E. G., 1996. "Wavenubmer space response of a near periodically ribbed shell". *Journal of the Acoustical Society of America,* **101(2)**, pp. 877–886.

[12] Atassi, H. M., Ali, A. A., Atassi, O. V., and Vinogradov, I. V., 2004. "Scattering of incident disturbances by an annular cascade in a swirling flow". *Journal of Fluid Mechanics,* **499**, pp. 111–138.

[13] Golubev, V. V., and Atassi, H. M., 1998. "Acoustic-vorticity waves in swirling flows". *Journal of Sound and Vibration,* **209**(2), pp. 203–222.

[14] Ali, A. A., 2001. "Aeroacoustics and stability of swirling flow". PhD thesis, University of Notre Dame.